ACS APPLIED MATERIALS & INTERFACES

Research Article

www.acsami.org

Organic Dyes Incorporating the Dithieno[3′,2′:3,4;2″,3″:5,6]benzo[1,2-*c*]furazan Moiety for Dye-Sensitized Solar Cells

Jen-Shyang Ni,[†] Jian-Hao You,[‡] Wei-I Hung,[†] Wei-Siang Kao,[†] Hsien-Hsin Chou,[†] and Jiann T. Lin*[,†,‡]

[†]Institute of Chemistry, Academia Sinica, Nankang, Taipei 115, Taiwan

[‡]Department of Chemistry, National Central University, Chungli 320, Taiwan

Supporting Information

ABSTRACT: New D−π−A′−π−A type sensitizers (JH dyes), comprised arylamine as the electron donor, dithieno[3′,2′:3,4;2″,3″:5,6]benzo[1,2-*c*]-furazan (DTBF) in the conjugated spacer, and 2-cyanoacrylic acid as both the acceptor and anchor, have been synthesized. The JH dyes have broad absorption spectra covering the range of 350 to 600 nm with the highest molar extinction coefficient up to >40 000 M^{-1} cm^{-1}. The dye-sensitized solar cells (DSSCs) fabricated from the dyes exhibited light-to-electricity conversions ranging from 1.42 to 6.18% under simulated AM 1.5 G illumination. Upon adding 10 mM CDCA as the coadsorbent, the best performance cell has the power conversion efficiency of 7.33%, which is close to that of N719-based standard DSSC (7.56%).

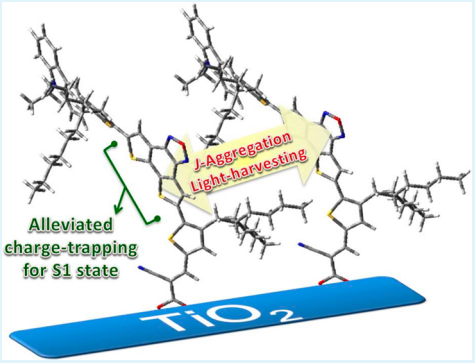

KEYWORDS: *dye-sensitized solar cells, organic sensitizer, benzo[1,2-c]furazan, J-aggregation, D−π−A′−π−A*

INTRODUCTION

Dye-sensitized solar cell (DSSC) has attracted vast attention due to its easy fabrication and high power conversion efficiency (PCE) feasible for commercial applications.[1,2] Over the past years, the major compositions of DSSCs, such as the photoelectrodes, dyes, electrolytes, and counter electrodes, have been investigated extensively aiming at better photovoltaic performance. Organic sensitizers can be divided into two mainstreams: metal complexes and metal-free dyes. For DSSCs using single dye, high power cell conversion efficiencies (PCEs) over 11.5%[3,4] and 12.8%,[5,6] have been achieved for ruthenium and zinc−porphyrin dyes, respectively. In comparison, a record high efficiency of 10.65%[7] was reported for a metal-free dye recently. Though with slightly lower efficiency, metal-free organic dyes drew great attention due to their lower cost, easy purification and more flexibility in molecular design. Prototype skeletons of metal-free dyes include D−π−A (D, donor; π, π-conjugated bridge; A, acceptor),[8] D−π−A′−π−A,[9−11] $(D)_2$−π−A,[12] and D−π−$(A)_2$.[13] D−π−A′−π−A type sensitizers with incorporation of an additional electron-withdrawing segment A′ in the conjugated spacer, such as benzothiadiazole,[14,15] benzoxadiazole,[16] benzotriazole,[10,17] benzothiazole,[18] diketopyrrolopyrrole (DPP),[19−21] thiadiazolo[3,4-*c*]-pyridine,[22,23] pyrido[3,4-*b*]pyrazine,[24] quinoxaline,[25,26] isoindigo,[27,28] thiazole,[29] cyano-,[30] and fluoro-substituted[31] phenyl, received considerable studies. The presence of the internal acceptor can significantly redshift the intramolecular charge-transfer absorption band and is beneficial to harvest sunlight of longer wavelength. A good example is DPP17 dye[21] based on DPP. Compared with the DPP moiety that absorbs at ∼460 nm with the molar extinction coefficient of ∼15 000 M^{-1} cm^{-1}, DPP17 absorbs at a significantly longer wavelength of 602 nm and an impressively high molar extinction coefficient of ∼69 000 M^{-1} cm^{-1}. On the other hand, the strong electron-withdrawing group may result in charge trapping in the conjugated spacer and hamper the electron injection efficiency of the excited dye molecule.[11]

In continuation of our studies on D−π−A′−π−A type sensitizers,[9−11] we decided to use dithieno[3′,2′:3,4;2″,3″:5,6]-benzo[1,2-*c*]furazan (DTBF)[32] entity, consisting of both electron-rich bithiophene and electron-deficient benzo[1,2-*c*]furazan units, as the internal acceptor based on the following reasons: (1) the planarized bithiophene entity in DTBF is beneficial to electronic communication between the donor and acceptor; (2) the electron-deficient benzo[1,2-*c*]furazan in DTBF is beneficial to red shifting the absorption spectrum; (3) the rigidity of DTBF may reduce reorganization energy of the dye molecule during photoexcitation. While the manuscript was in preparation, we were aware of a paper using a segment also containing both electron-rich and electron-deficient units, dithienopyrrolobenzothiadiazole (DTPBT).[33] Compared with an oxygen atom, a S atom in the conjugated spacer has stronger interaction with I_2 and/or I_3^- ions than an oxygen atom and leads to more dark currents.[34−36] Therefore, alleviation of dark

Received: September 30, 2014
Accepted: December 3, 2014
Published: December 3, 2014

current is expected with the use of DTBF. In this study, we synthesized a series of D−π−A′−π−A type sensitizers consisting aryl-amine as the donor, cyanoacetic acid as the acceptor, and DTBF as the internal acceptor. The photophysical and electrochemical properties of the dyes as well as their application for DSSCs will be discussed.

EXPERIMENTAL DETAILS

Materials. All chemicals were obtained from Alfa Lancaster, Acros and Aldrich. The solvents were dried over sodium or CaH_2 and distilled before use. The starting material 5,8-dibromodithieno-[3′,2′:3,4;2″,3″:5,6]benzo[1,2-*c*][1,2,5]oxadiazole (Br-DTBF-Br),[32] tri-*n*-butyl(3-(2-butyloctyl)thiophen-2-yl)stannane,[37] *N*,*N*-diphenyl-4-(tri-*n*-butylstannyl)aniline,[38] 10-ethyl-3-(tri-*n*-butylstannyl)-10*H*-phenothiazine, 9,9-diethyl-*N*,*N*-diphenyl-7-(tri-*n*-butylstannyl)-9*H*-fluoren-2-amine,[39] and 9-ethyl-3-(tri-*n*-butylstannyl)-9*H*-carbazole[40] were prepared according to the published procedures. TiO_2 paste was purchased from Solaronix S. A., Switzerland.

Synthesis of 5,8-bis(3-(2-butyloctyl)thiophen-2-yl)dithieno-[3′,2′:3,4;2″,3″:5,6]benzo[1,2-*c*][1,2,5]oxadiazole (1). Br-DTBF-Br (0.6 g, 1.5 mmol), $PdCl_2(PPh_3)_4$ (0.050 g, 8 mmol %), and tri-*n*-butyl(3-(2-butyloctyl)thiophen-2-yl)stannane (1.84 g, 3.4 mmol) were dissolved in 2.0 mL of dry DMF and stirred at 80 °C overnight. The solvent was removed under vacuum and then extracted with CH_2Cl_2 and deionized water. The combined organic layers were dried over anhydrous $MgSO_4$, evaporated and purified with column chromatography on silica gel using CH_2Cl_2/hexanes (1/4, v/v) as the eluent to give an orange solid (33% yield). ^{1}H NMR (400 MHz, $CDCl_3$): δ 7.88 (s, 2H), 7.29 (d, J_{HH} = 4.8 Hz, 2H), 6.96 (d, J_{HH} = 4.8 Hz, 2H), 2.78 (d, J_{HH} = 7.2 Hz, 4H), 1.71 (s, 2H), 1.23−1.16 (m, 32H), 0.81−0.79 (m, 12H). ^{13}C NMR (500 MHz, $CDCl_3$): δ 145.7, 140.9, 137.8, 136.0, 131.0, 129.5, 125.4, 122.6, 122.2, 39.2, 34.0, 33.6, 33.4, 32.0, 29.8, 28.9, 26.6, 23.2, 14.2. MS (MALDI, *m*/*z*): $[M-H]^+$ calcd for $C_{42}H_{56}N_2OS_4$, 733.2; found, 733.3.

Synthesis of 4-(2-butyloctyl)-5-(8-(3-(2-butyloctyl)thiophen-2-yl)dithieno [3′,2′:3,4;2″,3″:5,6]benzo[1,2-*c*][1,2,5]oxadiazol-5-yl)thiophene-2-carbaldehyde (2). Phosphoryl chloride (0.16 mL, 1.7 mmol) was added dropwise into a mixture of **1** (1.03 g, 1.4 mmol) and DMF (3.05 g, 24.4 mmol) solution cooled in an ice-bath. After being stirred for 30 min, the mixture was heated at 60 °C for 3 h. After cooling to room temperature (RT), a sodium acetate aqueous solution was added dropwise to the reaction mixture. The reaction mixture was then extracted with CH_2Cl_2, washed with brine, dried over $MgSO_4$, filtered, and then evaporated under reduced pressure. The residue was purified with column chromatography on silica gel using CH_2Cl_2/hexanes (1/2, v/v) as the eluent to give an orange solid (11% yield). ^{1}H NMR (400 MHz, $CDCl_3$): δ 9.88 (s, 1H), 8.02 (s, 1H), 7.89 (s, 1H), 7.61 (s, 1H), 7.31 (d, J_{HH} = 5.2 Hz, 1H), 6.97 (d, J_{HH} = 5.2 Hz, 1H), 2.82 (dd, J_{HH} = 7.2 Hz, 2H), 2.79 (dd, J_{HH} = 7.2 Hz, 2H), 1.72 (s, 1H), 1.23−1.17 (m, 32H), 0.86−0.78 (m, 12H). ^{13}C NMR (500 MHz, $CDCl_3$): δ 182.7, 145.7, 142.1, 141.8, 141.3, 139.3, 139.2, 138.8, 137.4, 135.6, 131.1, 129.3, 125.8, 124.0, 123.5, 122.8, 122.4, 39.2, 39.1, 34.1, 33.7, 33.6, 33.4, 33.3, 32.0, 29.8, 26.7, 23.1, 22.8, 14.2. MS (MALDI, *m*/*z*): $[M-H]^+$ calcd for $C_{43}H_{56}N_2O_2S_4$, 761.2; found, 761.2.

Synthesis of 5-(8-(5-bromo-3-(2-butyloctyl)thiophen-2-yl)-dithieno[3′,2′:3,4;2″,3″:5,6] benzo[1,2-*c*][1,2,5]oxadiazol-5-yl)-4-(2-butyloctyl)thiophene-2-carbaldehyde (3). To a solution of **2** (0.61 g, 0.8 mmol) in a mixture of dichloromethane and acetic acid (10 mL, v/v, 1/1) solution cooled in an ice-bath was added NBS (0.18 g, 1.0 mmol) in three portions in dark. After being stirred overnight at room temperature, the mixture was quenched with saturating $Na_2S_2O_3$ aqueous solution, and then extracted with CH_2Cl_2. The organic layer was dried over anhydrous $MgSO_4$ and concentrated under reduced pressure to give the crude product. The residue was purified by silica gel column chromatography using CH_2Cl_2/hexanes (1/5, v/v) as the eluent to afford a deep orange solid in 91% yield. ^{1}H NMR (400 MHz, $CDCl_3$): δ 9.88 (s, 1H), 8.02 (s, 1H), 7.84 (s, 1H), 7.61 (s, 1H), 6.93 (s, 1H), 2.81 (d, J_{HH} = 7.2 Hz, 1H), 2.71 (d, J_{HH} = 7.2 Hz, 1H), 1.65 (s, 2H), 1.23−1.17 (m, 32H), 0.83−0.78 (m, 12H). ^{13}C NMR (500 MHz, $CDCl_3$): δ 182.7, 145.6, 142.2, 142.1, 142.0, 139.2, 137.2, 136.1, 136.0, 135.9, 133.6, 130.7, 124.0, 123.4, 122.9, 113.0, 39.2, 39.1, 34.2, 34.1, 33.6, 33.5, 33.4, 32.0, 29.8, 29.7, 29.0, 26.7, 26.6, 23.1, 22.8, 14.2.

Synthesis of 5-(8-(5-(4-(diphenylamino)phenyl)-3-(2-butyloctyl)thiophen-2-yl)dithieno [3′,2′:3,4;2″,3″:5,6]benzo[1,2-*c*]-[1,2,5]oxadiazol-5-yl)-4-(2-butyloctyl)thiophene-2-carbaldehyde (4a). Compound **3** (0.51 g, 0.6 mmol), $PdCl_2(PPh_3)_4$ (0.020 g, 3 mmol %), and *N*,*N*-diphenyl-4-(tri-*n*-butylstannyl)aniline (0.50 g, 0.9 mmol) were dissolved in 2.0 mL of dry DMF and stirred at 80 °C overnight. The solvent was removed under vacuum and then extracted with CH_2Cl_2 and deionized water. The combined organic layers were dried over anhydrous $MgSO_4$ and evaporated, and the residue was purified with column chromatography on silica gel using CH_2Cl_2/hexanes (1/2, v/v) as the eluent to afford a red solid in 69% yield. ^{1}H NMR (400 MHz, $CDCl_3$): δ 9.88 (s, 1H), 8.02 (s, 1H), 7.90 (s, 1H), 7.61 (s, 1H), 7.45 (d, J_{HH} = 7.6 Hz, 2H), 7.29−7.25 (m, 4H), 7.12 (d, J_{HH} = 7.6 Hz, 4H), 7.07−7.03 (m, 5H), 2.83 (d, J_{HH} = 7.2 Hz, 2H), 2.79 (d, J_{HH} = 7.2 Hz, 2H), 1.75 (s, 1H), 1.25−1.19 (m, 32H), 0.84−0.80 (m, 12H). ^{13}C NMR (500 MHz, $CDCl_3$): δ 182.6, 148.0, 147.5, 145.6, 142.2, 142.0, 141.7, 139.4, 139.2, 139.0, 137.8, 137.4, 135.7, 135.0, 129.5, 127.4, 126.6, 126.1, 125.3, 124.9, 124.0, 123.9, 123.5, 123.4, 122.6, 122.5, 121.6, 39.1, 34.5, 34.2, 33.6, 33.5, 33.4, 32.0, 31.9, 29.8, 29.7, 28.9, 26.7, 23.2, 23.1, 22.8, 14.2. MS-LR-MALDI (*m*/*z*): $[M + H]^+$ calcd for $C_{61}H_{69}N_3O_2S_4$, 1004.5; found, 1004.4.

Synthesis of 4-(2-butyloctyl)-5-(8-(3-(2-butyloctyl)-5-(10-ethyl-10*H*-phenothiazin-3-yl)thiophen-2-yl)dithieno-[3′,2′:3,4;2″,3″:5,6]benzo[1,2-*c*][1,2,5]oxadiazol-5-yl)-thiophene-2-carbaldehyde (4b). The synthetic method was similar to that of **4a** except that *N*,*N*-diphenyl-4-(tri-*n*-butylstannyl)aniline was replaced with 10-ethyl-3-(tri-*n*-butylstannyl)-10*H*-phenothiazine. Compound **4b** was isolated as a red solid in 38% yield. ^{1}H NMR (400 MHz, $CDCl_3$): δ 9.87 (s, 1H), 7.99 (s, 1H), 7.87 (s, 1H), 7.59 (s, 1H), 7.34−7.31 (m, 2H), 7.16−7.10 (m, 2H), 7.02 (s, 1H), 6.91 (t, J_{HH} = 7.2 Hz, 1H), 6.86 (d, J_{HH} = 8.0 Hz, 1H), 6.82 (d, J_{HH} = 8.0 Hz, 1H), 3.92 (q, J_{HH} = 7.2 Hz, 2H), 2.82 (d, J_{HH} = 7.2 Hz, 1H), 2.76 (d, J_{HH} = 7.2 Hz, 1H), 1.75 (s, 1H), 1.74 (s, 1H), 1.42 (t, J_{HH} = 7.2 Hz, 3H), 1.25−1.18 (m, 32H), 0.85−0.78 (m, 12H). ^{13}C NMR (500 MHz, $CDCl_3$): δ 182.7, 145.7, 144.9, 144.5, 143.2, 142.2, 142.0, 141.7, 139.4, 139.2, 138.9, 137.4, 135.7, 135.1, 128.0, 127.6, 126.1, 125.1, 124.9, 124.3, 124.0, 123.7, 122.8, 121.7, 115.3, 42.1, 39.1, 34.5, 34.2, 33.7, 33.6, 33.5, 33.4, 32.1, 32.0, 29.8, 29.0, 28.9, 26.7, 23.2, 23.1, 22.8, 14.2, 13.1. MS-LR-MALDI (*m*/*z*): $[M + H]^+$ calcd for $C_{57}H_{67}N_3O_2S_5$, 986.5; found, 986.4.

Synthesis of 4-(2-butyloctyl)-5-(8-(3-(2-butyloctyl)-5-(7-(diphenylamino)-9,9-diethyl-9*H*-fluoren-2-yl)thiophen-2-yl)-dithieno[3′,2′:3,4;2″,3″:5,6]benzo[1,2-*c*][1,2,5]oxadiazol-5-yl)-thiophene-2-carbaldehyde (4c). The synthetic method was similar to that of **4a** except that *N*,*N*-diphenyl-4-(tri-*n*-butylstannyl)aniline was replaced with 9,9-diethyl-*N*,*N*-diphenyl-7-(tri-*n*-butylstannyl)-9*H*-fluoren-2-amine. Compound **4c** was isolated as a red solid in 58% yield. ^{1}H NMR (400 MHz, $CDCl_3$): δ 9.89 (s, 1H), 8.03 (s, 1H), 7.94 (s, 1H), 7.62−7.61 (m, 2H), 7.58 (s, 1H), 7.56 (d, J_{HH} = 8.0 Hz, 1H), 7.50 (s, 1H), 7.25 (t, J_{HH} = 8.0 Hz, 2H), 7.23−7.21 (m, 2H), 7.12 (d, J_{HH} = 8.0 Hz, 2H), 7.09 (sd, d, J_{HH} = 1.6 Hz, 2H), 7.04−6.99 (m, 5H), 2.83 (d, J_{HH} = 7.2 Hz, 4H), 1.98 (q, J_{HH} = 7.2 Hz, 2H), 1.90 (q, J_{HH} = 7.2 Hz, 2H), 1.82−1.79 (m, 1H), 1.75−1.73 (m, 1H), 1.28−1.20 (m, 32H), 0.85−0.80 (m, 12H), 0.51−0.44 (m, 6H). ^{13}C NMR (500 MHz, $CDCl_3$): δ 182.7, 151.7, 151.0, 148.1, 147.7, 145.7, 145.1, 142.3, 142.1, 141.8, 139.4, 139.2, 139.0, 137.5, 135.8, 135.2, 131.7, 129.4, 126.5, 124.9, 124.1, 124.0, 123.7, 122.8, 121.8, 120.7, 120.0, 119.7, 119.3, 39.2, 34.5, 34.2, 33.7, 33.5, 33.4, 32.8, 32.1, 32.0, 29.9, 29.8, 29.0, 26.7, 23.2, 23.1, 22.8, 14.2, 8.8. MS-LR-MALDI (*m*/*z*): $[M + H]^+$ calcd for $C_{72}H_{81}N_3O_2S_4$, 1148.7; found, 1148.5.

Synthesis of 4-(2-butyloctyl)-5-(8-(3-(2-butyloctyl)-5-(9-ethyl-9*H*-carbazol-3-yl)thiophen-2-yl)dithieno-[3′,2′:3,4;2″,3″:5,6]benzo[1,2-*c*][1,2,5]oxadiazol-5-yl)-thiophene-2-carbaldehyde (4d). The synthetic method was similar to that of **4a** except that *N*,*N*-diphenyl-4-(tri-*n*-butylstannyl)aniline was replaced with 9-ethyl-3-(tri-*n*-butylstannyl)-9*H*-carbazole. Compound **4d** was isolated as a red solid in 36% yield. ^{1}H NMR (400

MHz, $CDCl_3$): δ 9.85 (s, 1H), 8.20 (s, 1H), 8.07 (d, J_{HH} = 8.0 Hz, 1H), 7.91 (s, 1H), 7.85 (s, 1H), 7.65 (d, J_{HH} = 8.4 Hz, 1H), 7.56 (s, 1H), 7.45 (d, J_{HH} = 7.6 Hz, 1H), 7.36 (d, J_{HH} = 8.0 Hz, 1H), 7.32 (d, J_{HH} = 8.4 Hz, 1H), 7.21 (d, J_{HH} = 7.6 Hz, 1H), 7.14 (s, 1H), 4.34−4.28 (q, 2H), 2.82−2.78 (m, 4H), 1.82 (s, 1H), 1.73 (s, 1H), 1.42 (t, J_{HH} = 7.2 Hz, 3H), 1.34−1.21 (m, 32H), 0.88−0.79 (m, 12H). ^{13}C NMR (500 MHz, $CDCl_3$): δ 182.6, 145.6, 142.1, 141.8, 141.6, 140.5, 139.9, 139.5, 139.2, 137.4, 135.5, 134.7, 127.6, 126.3, 125.8, 124.8, 123.9, 123.8, 123.6, 123.5, 122.9, 122.4, 121.3, 129.7, 119.4, 117.7, 108.8, 39.1, 39.0, 37.8, 34.6, 34.2, 33.7, 33.6, 33.5, 32.1, 32.0, 29.9, 29.8, 29.0, 28.9, 26.7, 26.6, 23.2, 23.1, 22.8, 14.2. MS-LR-MALDI (m/z): $[M]^+$ calcd for $C_{57}H_{67}N_3O_2S_4$, 953.4; found, 953.4.

Synthesis of *(E)*-3-(4-(2-butyloctyl)-5-(8-(3-(2-butyloctyl)-5-(4-(diphenylamino)phenyl)-thiophen-2-yl)dithieno-[3′,2′:3,4;2″,3″:5,6]benzo[1,2-*c*][1,2,5]oxadiazol-5-yl)thiophen-2-yl)-2-cyanoacrylic acid (JH-1). Compound **4a** (0.12 g, 0.12 mmol), cyanoacetic acid (0.02 g, 0.24 mmol), ammonium acetate (3 mg, 0.04 mmol) were dissolved in 2.0 mL of acetic acid. The reaction mixture was then vigorously stirred at 120 °C for 20 h. The solution was cooled to RT and then poured into water. The precipitate was filtered, washed with deionized water, dried under vacuum, and purified with column chromatography on silica gel using acetic acid/ethyl acetate (1/100, v/v) as the eluent to give a purple solid in 60% yield. ^{1}H NMR (400 MHz, d_8−THF): δ 8.35 (s, 1H), 8.22 (s, 1H), 8.02 (s, 1H), 7.82 (s, 1H), 7.53 (d, J_{HH} = 8.0 Hz, 2H), 7.27−7.25 (m, 5H), 7.11−7.05 (m, 8H), 2.71 (d, J_{HH} = 7.2 Hz, 2H), 2.66 ((d, J_{HH} = 7.2 Hz, 2H), 1.90 (s, 2H), 1.25−1.19 (m, 32H), 0.83−0.80 (m, 12H). ^{13}C NMR (500 MHz, d_8−THF): δ 162.4, 152.7, 148.2, 147.7, 145.7, 142.3, 142.0, 141.8, 139.4, 139.2, 139.0, 137.8, 137.4, 135.7, 135.0, 129.5, 127.4, 126.6, 126.1, 125.3, 124.9, 124.0, 123.9, 123.5, 122.6, 122.5, 121.6, 39.1, 34.5, 34.2, 33.6, 33.5, 33.4, 32.0, 31.9, 29.8, 28.9, 26.6, 23.2, 23.1, 22.8, 14.2. MS-HR-MALDI (m/z): $[M]^+$ calcd for $C_{64}H_{70}N_4O_3S_4$, 1070.4331; found, 1070.4321. Anal. calcd for $C_{60}H_{70}N_4O_3S_4$: C, 71.74; H, 6.58; N, 5.23; found: C, 71.52; H, 6.61; N, 5.09.

Synthesis of *(E)*-3-(4-(2-butyloctyl)-5-(8-(3-(2-butyloctyl)-5-(10-ethyl-10*H*-phenothiazin-3-yl)thiophen-2-yl)dithieno-[3′,2′:3,4;2″,3″:5,6]benzo[1,2-*c*][1,2,5]oxadiazol-5-yl)-thiophen-2-yl)-2-cyanoacrylic acid (JH-2). The synthetic method was similar to that of JH-1 and JH-2 was isolated as a purple solid in 38% yield. ^{1}H NMR (400 MHz, d_8−THF): δ 8.31 (s, 1H), 8.11 (s, 1H), 7.92 (s,1H), 7.76 (s, 1H), 7.38−7.36 (m, 2H), 7.21 (s, 1H), 7.14 (t, J_{HH} = 8.0 Hz, 1H), 7.10 (d, J_{HH} = 7.6 Hz, 1H), 6.94 (d, J_{HH} = 8.0 Hz, 1H), 6.91−6.88 (m, 2H), 3.89 (t, J_{HH} = 6.8 Hz, 2H), 2,90 (d, J_{HH} = 6.8 Hz, 2H), 2.84 (d, J_{HH} = 6.8 Hz, 2H), 1.77 (s, 2H), 1.33−1.22 (m, 35H), 0.88−0.81 (m, 12H). ^{13}C NMR (500 MHz, d_8−THF): δ 162.9, 152.5, 145.7, 144.9, 144.6, 143.3, 142.2, 142.0, 139.3, 139.2, 138.9, 137.4, 135.7, 135.1, 128.1, 127.6, 126.1, 125.2, 124.9, 124.0, 123.7, 123.6, 122.8, 121.7, 115.3, 43.5, 39.2, 34.5, 34.2, 33.7, 33.6, 33.5, 32.0, 29.9, 29.8, 29.0, 28.9, 26.7, 23.2, 23.1, 22.8, 14.2. MS-HR-MALDI (m/z): $[M]^+$ calcd for $C_{60}H_{68}N_4O_3S_5$, 1052.3895; found, 1052.3896. Anal. calcd for $C_{60}H_{68}N_4O_3S_5$: C, 68.40; H, 6.51; N, 5.32; found: C, 68.20; H, 6.63; N, 5.18.

Synthesis of *(E)*-3-(4-(2-butyloctyl)-5-(8-(3-(2-butyloctyl)-5-(7-(diphenylamino)-9,9-diethyl-9*H*-fluoren-2-yl)thiophen-2-yl)-dithieno[3′,2′:3,4;2″,3″:5,6]benzo[1,2-*c*][1,2,5]oxa-diazol-5-yl)-thiophen-2-yl)-2-cyanoacrylic acid (JH-3). The synthetic method was similar to that of JH-1 and the crude product was purified with column chromatography on silica gel using ethyl acetate/dichloromethane (1/1, v/v) as the eluent to give JH-3 as a purple solid in 45% yield. ^{1}H NMR (400 MHz, d_8−THF): δ 8.37 (s, 1H), 8.25 (s, 1H), 8.09 (s, 1H), 7.84 (s, 1H), 7.73−7.64 (m, 4H), 7.43 (s, 1H), 7.26−7.22 (m, 4H), 7.14 (s, 1H), 7.10 (d, J_{HH} = 8.0 Hz, 4H), 7.04−6.94 (m, 3H), 2.96−2.93 (m, 4H), 2.08−2.03 (m, 2H), 1.99−1.95 (m, 2H), 1.35−1.22 (m, 32H), 0.88−0.83 (m, 12H), 0.40 (t, J_{HH} = 7.2 Hz, 2H). ^{13}C NMR (500 MHz, d_8−THF): δ 163.1, 153.8, 152.0, 151.1, 148.1, 147.7, 145.7, 145.1, 142.3, 142.1, 141.8, 139.4, 139.2, 139.0, 137.5, 135.8, 135.2, 131.7, 129.4, 126.6, 124.9, 124.1, 124.0, 123.7, 122.7, 121.8, 120.7, 120.0, 119.7, 119.3, 39.2, 34.5, 34.2, 33.7, 33.5, 33.4, 32.8, 32.1, 32.0, 29.9, 29.8, 26.7, 23.2, 23.1, 22.8, 14.2, 8.8. MS-HR-MALDI (m/z): $[M]^+$ calcd for $C_{75}H_{82}N_4O_3S_4$, 1214.5270; found, 1214.5276. Anal. calcd for $C_{75}H_{82}N_4O_3S_4$: C, 74.10; H, 6.80; N, 4.61; found: C, 74.29; H, 6.83; N, 4.70.

Synthesis of *(E)*-3-(4-(2-butyloctyl)-5-(8-(3-(2-butyloctyl)-5-(9-ethyl-9*H*-carbazol-3-yl)thiophen-2-yl)dithieno-[3′,2′:3,4;2″,3″:5,6]benzo[1,2-*c*][1,2,5]oxadiazol-5-yl)-thiophen-2-yl)-2-cyanoacrylic acid (JH-4). The synthetic method was similar to that of JH-1 and the crude product was purified with column chromatography on silica gel using ethyl acetate/dichloromethane (1/1, v/v) as the eluent to give JH-4 as a purple solid in 25% yield. ^{1}H NMR (400 MHz, $CDCl_3$): δ 8.25 (s, 1H), 8.13 (s, 1H), 8.07 (d, J_{HH} = 8.0 Hz, 1H), 7.96 (s, 1H), 7.80 (s, 1H), 7.72−7.70 (m, 2H), 7.57 (t, J_{HH} = 8.0 Hz, 1H), 7.42 (d, J_{HH} = 8.0 Hz, 1H), 7.39 (t, J_{HH} = 8.0 Hz, 1H), 7.20 (d, J_{HH} = 8.0 Hz, 1H), 7.12 (s, 1H), 4.34−4.28 (q, 2H), 2.83−2.78 (m, 4H), 1.82 (s, 1H), 1.73 (s, 1H), 1.42 (t, J_{HH} = 7.2 Hz, 3H), 1.34−1.21 (m, 32H), 0.88−0.79 (m, 12H). ^{13}C NMR (500 MHz, d_8−THF): δ 163.8, 153.5, 148.8, 147.4, 145.7, 142.2, 141.9, 141.6, 140.6, 139.9, 139.5, 139.2, 127.6, 125.9, 124.8, 123.9, 123.6, 122.9, 121.3, 120.7, 119.4, 117.7, 109.2, 41.6, 39.8, 34.7, 33.7, 33.6, 33.5, 33.4, 32.1, 32.0, 29.9, 29.0, 28.9, 26.7, 26.7, 23.2, 23.1, 22.8, 14.2. MS-HR-MALDI (m/z): $[M]^+$ calcd for $C_{60}H_{68}N_4O_3S_4$, 1020.4174; found, 1020.4178. Anal. calcd for $C_{60}H_{68}N_4O_3S_4$: C, 70.55; H, 6.71; N, 5.48; found: C, 70.47; H, 6.83; N, 5.32.

Fabrication of DSSC. Dye-sensitized solar cells were fabricated using fluorine-doped tin oxide (FTO, 15Ω/square) glasses as substrate for photoanode and counter electrode. The counter electrode was fabricated by depositing a thin Pt layer with sputtering. The photoanode used was the TiO_2 thin film (12 μm of 20 nm particles as the absorbing layer and 6 μm of 100 nm particles as the scattering layer) coated on FTO glass substrate with a dimension of 0.4 × 0.4 cm^2 as the active area. The film thickness was measured by a profilometer (Dektak3, Veeco/Sloan Instruments Inc., U.S.A.). The TiO_2 thin film was immersed into the THF solution containing 0.3 mM dye sensitizers and with or without 10 mM chenodeoxycholic acid (CDCA) as the coadsorbent, for 12 h. After rinsing with THF, the photoanode adhered with a polyimide tape of 30 μm in thickness and with a square aperture of 0.36 cm^2 was placed on top of the counter electrode and tightly clipping them together to form a cell. Electrolyte was then injected into the seam between two electrodes. The liquid electrolytes containing 0.5 M lithium iodide (LiI), 0.05 M iodine (I_2), and 0.5 M 4-*tert*-butylpyridine in acetonitrile were prepared.

Analytical Methods. ^{1}H and ^{13}C nuclear magnetic resonance (NMR) spectra were recorded on a Bruker Avance 400 and 500 MHz spectrometer by utilizing deuterated tetrahydrofuran (d_8−THF) and $CDCl_3$ as solvents. Mass spectra (MALDI) were recorded on a 4800 MALDI TOF/TOF analyzer. Elementary analyses were performed on a PerkinElmer 2400 CHN analyzer. Absorption spectra were recorded on a Dynamica DB-20 probe UV/vis spectrophotometer. Fluorescence spectra were recorded on a Hitachi F-4500 spectrophotometer. Cyclic voltammetry experiments were performed with a CHI-621A electrochemical analyzer. All measurements were carried out at room temperature with a conventional three electrode configuration consisting of a platinum working electrode, an auxiliary electrode and a nonaqueous $Ag/AgNO_3$ reference electrode. The photoelectrochemical characterizations on the solar cells were carried out using an Oriel Class AAA solar simulator (Oriel 94043 A, Newport Corp.). Photocurrent−voltage characteristics of the DSSCs were recorded with a potentiostat/galvanostat (CHI650B, CH Instruments, Inc.) at a light intensity of 100 mW/cm^2 calibrated by an Oriel reference solar cell (Oriel 91150, Newport Corp.). The monochromatic quantum efficiency was recorded through a monochromator (Oriel 74100, Newport Corp.) at short circuit condition, and the monochromator was scanned through the UV−vis region to generate the IPCE plots as defined by IPCE = $1240(J_{sc}/\omega\lambda)$, where J_{sc} is the short-circuit photocurrent (mA/cm^2), ω is the incident irradiative flux (W/cm^2), and λ is the wavelength. The intensity of each wavelength was in the range from 1 to 3 mW/cm^2. Electrochemical impedance spectra (EIS) were recorded for DSSC under illumination at open-circuit voltage (V_{oc}) or dark at −0.55 V potential at room temperature. The frequencies explored ranged from 10 mHz to 100 kHz.

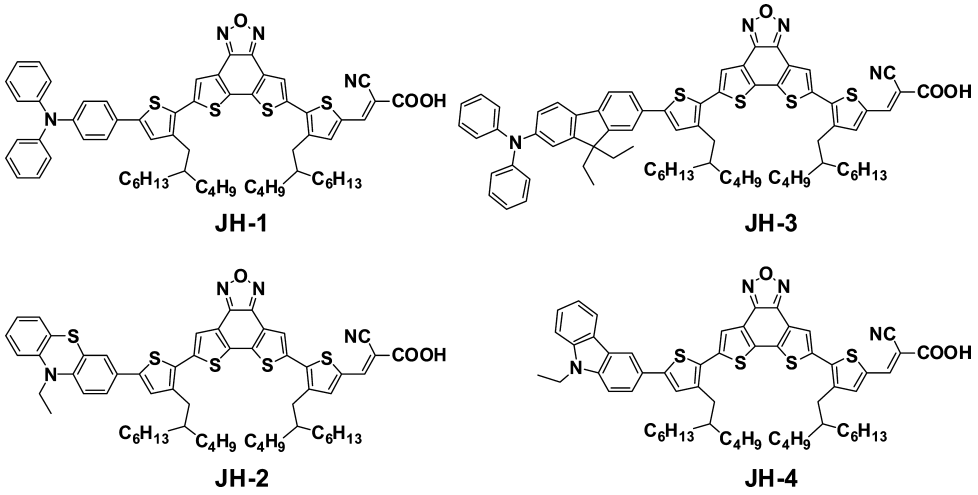

Figure 1. Structures of JH dyes.

Scheme 1. Synthetic Route of JH Dyes

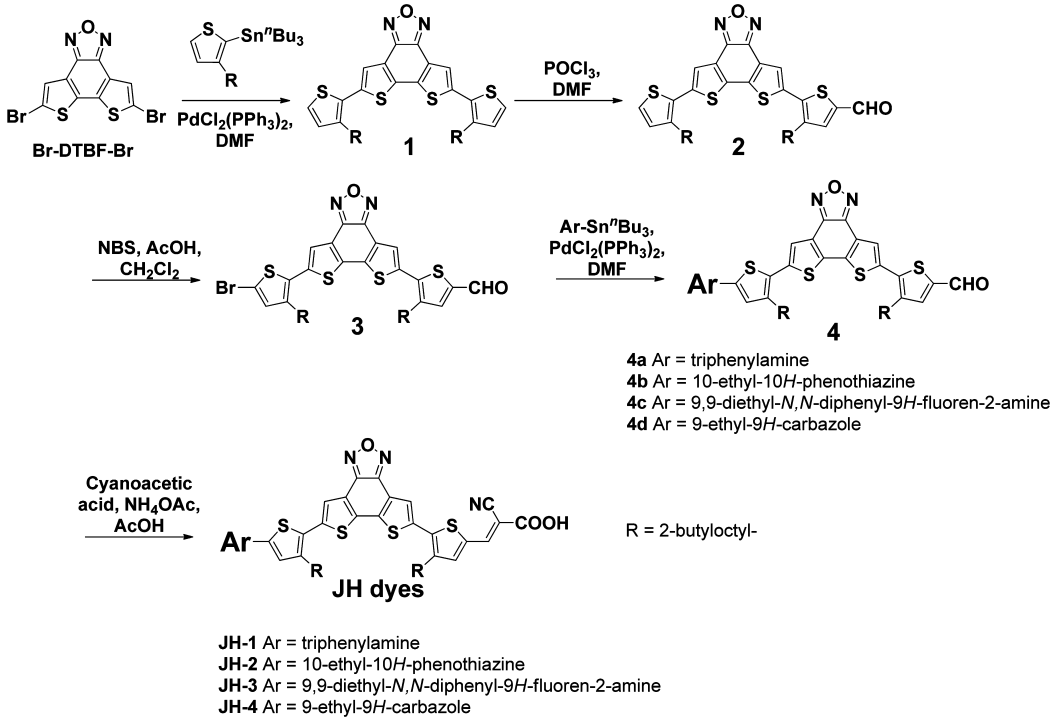

Quantum Chemistry Computation. The computation was performed with Q-Chem4.0 software. B3LYP functional level and 6-31G* basis set was used for optimization of molecular geometry. A number of possible conformations were examined for each molecule and the one with the lowest energy was used. The excited states were calculated using time-dependent density functional theory (TD−DFT) with the same functional level. There exist a number of previous works that employed TD−DFT to characterize excited states with charge-transfer character.[41,42] In some cases underestimation of the excitation energies was seen.[43] Therefore, TD−DFT was used to visualize the extent of transition moments as well as their charge-transfer characters without drawing conclusions from the excitation energy.

RESULTS AND DISCUSSION

Design and Synthesis of JH Dyes. The structures of new DTBF-based dyes are shown in Figure 1, and the synthetic routes of the compounds are depicted in Scheme 1. The starting material, 5,8-dibromodithieno[3′,2′:3,4;2″,3″:5,6]-benzo[1,2-*c*][1,2,5]oxadiazole (Br-DTBF-Br) was prepared from DTBF with NBS, similar to the published procedures.[17,32] The Pd-catalyzed Stille cross-coupling[44] of Br-DTBF-Br with 2-butyloctyl-thiophen-2-yl stannane in refluxing DMF afforded compound **1** in 33% yield. Subsequent formylation using Vilsmeier−Haack reagent and bromination using NBS generated **3**. Intermediate **4** was then obtained from Pd-catalyzed Stille cross-coupling of **3** with stannyl derivatives: *N*,*N*-diphenyl-4-(tri-*n*-butylstannyl)-aniline[38] for **4a**, 10-ethyl-3-(tri-*n*-butylstannyl)-10*H*-phenothiazine for **4b**, 9,9-diethyl-*N*,*N*-diphenyl-7-(tri-*n*-butylstannyl)-9*H*-fluoren-2-amine[39] for **4c**, and 9-ethyl-3-(tri-*n*-butylstannyl)-9*H*-carbazole[40] for **4d**. Finally, Knoevenagel condensation of **4** with cyanoacetic acid produced the desired dyes, JH-1−JH-4. The new organic dyes

were characterized by NMR, mass spectra, and elemental analysis.

UV−Vis Absorption Properties of JH Dyes. UV−vis absorption spectra of JH dyes in THF are shown in Figure 2,

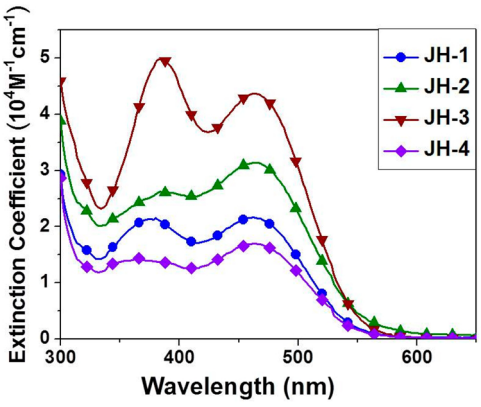

Figure 2. UV−vis absorption spectra of JH dyes in THF solutions of 10 μM concentration.

and the corresponding data are summarized in Table 1. The high energy absorption peaks between 366 and 380 nm are assigned to the $\pi-\pi^*$ transitions, whereas the low energy peak at 462 and 464 nm are attributed to the intramolecular charge transfer (ICT) transitions.[41] Due to the large dimension of DTBF, incorporating the long hydrocarbon chains at the thienyl rings is necessary for good solubility of the dyes in common organic solvents and suppression of dye aggregation. However, the presence of these chains leads to large dihedral angles (33.1−44.2°, vide infra) between DTBF and the neighboring thienyl ring, which jeopardizes the electronic communication between the donor and the acceptor. Therefore, the absorption maximum of the ICT band does not differ much among the dyes. JH-3 has an impressively high molar extinction coefficient (ε) of 4.37×10^4 $M^{-1}cm^{-1}$ at 462 nm due to its elongated conjugation.

Compared with the solution spectra, there is red shift of the absorption spectra (Supporting Information Figure S1 and Table 1) for the dyes adsorbed on the TiO_2 film, which can be ascribed to the formation of *J*-aggregation.[45] Though dye aggregation normally jeopardizes electron injection, there are some examples illustrating that *J*-aggregation could improve the cell performance due to improved light harvesting at longer wavelengths.[46,47] Aggregation of the dye molecules was also supported by examining the spectra of the JH dyes adsorbed on TiO_2 film with and without the coabsorbent, CDCA (Supporting Information Figure S2). Addition of ~30 fold (10 mM) of CDCA resulted in blue shift of $\lambda_{abs}(TiO_2)$ by about 6, 18, 12, and 6 nm for JH-1, JH-2, JH-3, and JH-4, respectively. However, aggregation of JH dyes still remained, as evidenced from the incident photon-to-current conversion efficiency (IPCE) plots of DSSCs fabricated with CDCA coadsorbent (vide infra).

Electrochemical Properties. The electrochemical properties of the organic dyes were measured by cyclic voltammetry (CV) in THF solutions at a concentration of 1 mM (Supporting Information Figure S4), and the relevant data are listed in Table 1. A quasi-reversible one-electron oxidation is attributed to the removal of electron from the arylamine. The HOMO (highest occupied molecular orbital) energy levels of the compounds were calculated from the first oxidation potential and by comparison with ferrocene (5.1 eV),[48] which was followed by the equation, $E_{HOMO} = 5.1 + E_{1/2}(ox)$. The lowest unoccupied molecular orbital (LUMO) was obtained from the value of E_{ox} and the zero−zero band gap (E_{0-0}) according to the equation $E_{LUMO} = E_{HOMO} - E_{0-0}$,[49] where E_{0-0} was estimated from the intersection of the absorption and emission spectra of the dye (Suppporting Information Figure S3). The first quasi-reversible one-electron oxidation wave detected at about 288−566 mV more positive than ferrocene/ferrocenium (F_c/F_c^+) is attributed to the removal of electron from the arylamine donor. This potential decreases in the order of JH-4 > JH-1 > JH-3 > JH-2, which is consistent with the electron-donating power of the donor (phenothiazine the strongest and carbazole the weakest) and the influence of nearby thiophene on the arylamine (JH-1 is larger than JH-3). The excited state potential (E_{0-0}*) of the sensitizer, estimated from the difference between the first oxidation potential at the ground state and the zero−zero excitation energy E_{0-0} obtained from the intersection of the normalized absorption and emission spectra, ranges from −1.07 to −1.36 V (vs NHE). Therefore, electron injection from the excited dye into the conduction band of TiO_2 (conduction band edge: −0.5 V vs NHE)[50] is energetically favorable. The first oxidation potentials of the dyes (0.99 to 1.27 V vs NHE, see Table 1) are more positive than that of the I^-/I_3^- redox couple (0.4 V vs NHE),[19] suggesting that dye regeneration should also be energetically favorable. The least driving force for the dye regeneration due to the highest HOMO energy level may be the cause of the low cell performance of JH-2 (vide infra).

Theoretical Approach. Density functional theory (DFT) as well as time-dependent DFT calculations at B3LYP/6-31G* level using Q-Chem4.0 software were carried on the dye molecules in order to correlate the molecular structures of the dyes with the performance of DSSCs. The results for the time-dependent approach are summarized in Supporting Informa-

Table 1. Electro-Optical Parameters of the Dyes

dye	λ_{abs} ($\varepsilon \times 10^4$ M^{-1} cm^{-1}) (nm)[a]	λ_{em} (nm)[a]	$\lambda_{abs}(TiO_2)$ (nm)[b]	E_{0-0} (eV)[c]	$E_{1/2}(ox)$ (ΔE_p) (mV)[d]	E_{ox} (V)[e]	E_{0-0}* (V)[e]	HOMO/LUMO (eV)[f]
JH-1	380 (2.16), 462 (2.17)	658	484	2.38	541 (181)	1.24	−1.14	−5.64/−3.26
JH-2	390 (2.61), 464 (3.14)	690	504	2.35	288 (147)	0.99	−1.36	−5.39/−3.05
JH-3	386 (4.99), 462 (4.37)	698	486	2.34	466 (113)	1.17	−1.17	−5.57/−3.23
JH-4	366 (1.44), 462 (1.70)	702	476	2.34	566 (184)	1.27	−1.07	−5.67/−3.33

[a]Recorded in THF solutions at 298 K. [b]Recorded on the TiO_2 film. [c]The band gap, E_{0-0}, calculated from the onset of UV−vis absorption spectrum. [d]Recorded in THF. Scan rate: 100 mV/s. Electrolyte: $(n\text{-}C_4H_9)_4NPF_6$. ΔE_p: separation between the anodic and cathodic peaks. Potentials are quoted with reference to the internal ferrocene standard ($E_{1/2}$ = +265 mV vs $Ag/AgNO_3$). [e]E_{ox}: The oxidation potential vs NHE, E_{Fc} = 0.7 V vs NHE. E_{0-0}*: the excited state oxidation potential vs NHE, $E_{0-0}^* = E_{ox} + E_{0-0}$. [f]HOMO and LUMO energies are calculated using formula HOMO = −[5.1 + ($E_{1/2}$ − E_{Fc})], LUMO = −[E_{0-0} − HOMO].

dx.doi.org/10.1021/am5067145 | ACS Appl. Mater. Interfaces 2014, 6, 22612−22621

tion Table S1. Selected frontier orbitals of the dyes are shown in Figure 3 and Supporting Information Figure S5. The

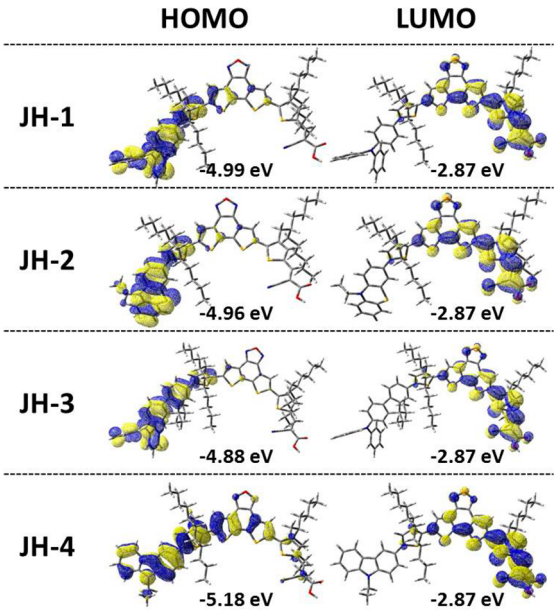

Figure 3. Frontier molecular orbitals of the dyes.

HOMO in these compounds is mainly distributed from donor group to the conjugated spacer. In comparison, the LUMO and LUMO+1 are largely distributed from 2-cyano acrylic acid (Ac) to the spacer, and the DTBF core has more contribution to the latter. The lowest energy transition ($S_0 \rightarrow S_1$) is ~100% of HOMO → LUMO transition for all the compounds. In comparison, the $S_0 \rightarrow S_2$ transitions mainly stem from HOMO−1 → LUMO and HOMO → LUMO+1 transitions. Both $S_0 \rightarrow S_1$ and $S_0 \rightarrow S_2$ transitions confirm the charge transfer character of the low energy band in the absorption spectra.

The ground-state intramolecular dihedral angles between the DTBF core and the neighboring thiophene rings, are shown in Supporting Information Figure S6. They range from 33.1 to 44.2°, which certainly will downgrade the charge transfer from the donor to the acceptor. This is believed to be the main cause that the JH dyes have similar absorption maximum (vide supra).

Mulliken charges variation during electronic transition was also calculated from the time-dependent DFT (TD-DFT) results,[51] as shown in Supporting Information Table S1. The molecules were divided into five segments: the donor group (DG, such as TPA, Ptz, DPAF and Cbz), the thiophene (T) between DG and DTBF, DTBF, the thiophene (T′) between DTBF and the acceptor, 2-cyanoacrylic acid (Ac). The Mulliken charges for the S1 and S2 states are shown in Figure 4. For comparison, Mulliken charge analysis was also carried out on JH-0 dye (Supporting Information Figure S6) containing an electron-deficient benzo[1,2-*c*]furazan (BF) entity. There is significant charge trapping at the BF of JH-0. In comparison, charge trapping at the DTBF of JH dyes has been largely alleviated for S1 state, which is beneficial to electron injection.

Photocurrent−Voltage Characteristics. The photocurrent density−voltage (J−V) characteristic plots and incident photon-to-current conversion efficiencies (IPCE) of DSSC with JH dyes and liquid electrolyte containing 0.50 M LiI, 0.05 M I_2, and 0.5 M TBP in acetonitrile under AM 1.5 full sunlight (100 mW/cm^2) illumination are shown in Figure 5, and the relevant cell performance data are listed in Table 2. The DSSCs of JH dyes exhibited good power conversion efficiencies (5.27−6.18%) except for JH-2 (1.42%). Though JH-2 has higher dye density (Table 2) on TiO_2 compared with other dyes, it has the lowest cell conversion efficiency, open-circuit voltage, and short circuit current among all. The low performance of JH-2 is likely stemmed from several factors: (1) JH-2 is less effective in blocking the electrolytes from approaching the TiO_2 surface, resulting in a higher dark current (Figure 5a) and lower open-circuit voltage (V_{oc}); (2) JH-2 has high-lying HOMO level, which slowdowns dye regeneration and leads to more facile charge recombination with the oxidized dye;[52] (3) the cell of JH-2 has slower electron transport (see electrochemical impedance spectroscopy (EIS) under illumination, vide infra) and/or slower electron injection.

The IPCE spectra of the DSSC (Figure 5b) with JH dyes extend to >650 nm, suggesting that *J*-aggregation of the dyes (Supporting Information Figure S1) contributes positively to the cell performance. Such phenomenon has precedents in literature.[46,47]

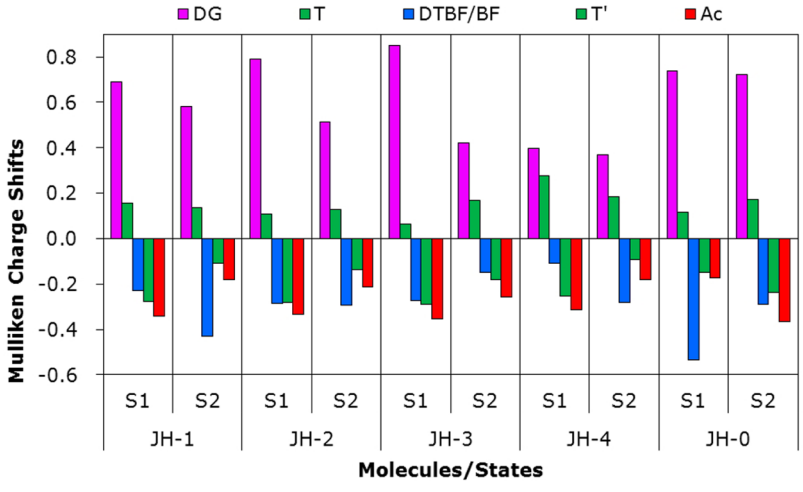

Figure 4. Plot of difference in Mulliken charge between ground state and excited state for dyes.

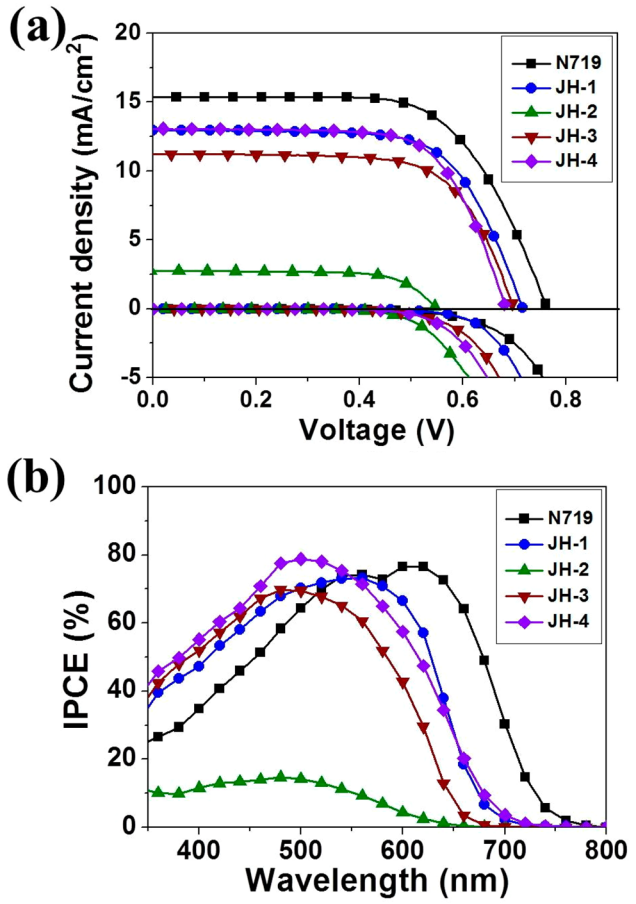

Figure 5. *J*−*V* curves (a) and IPCE plots (b) of DSSCs based on the dyes.

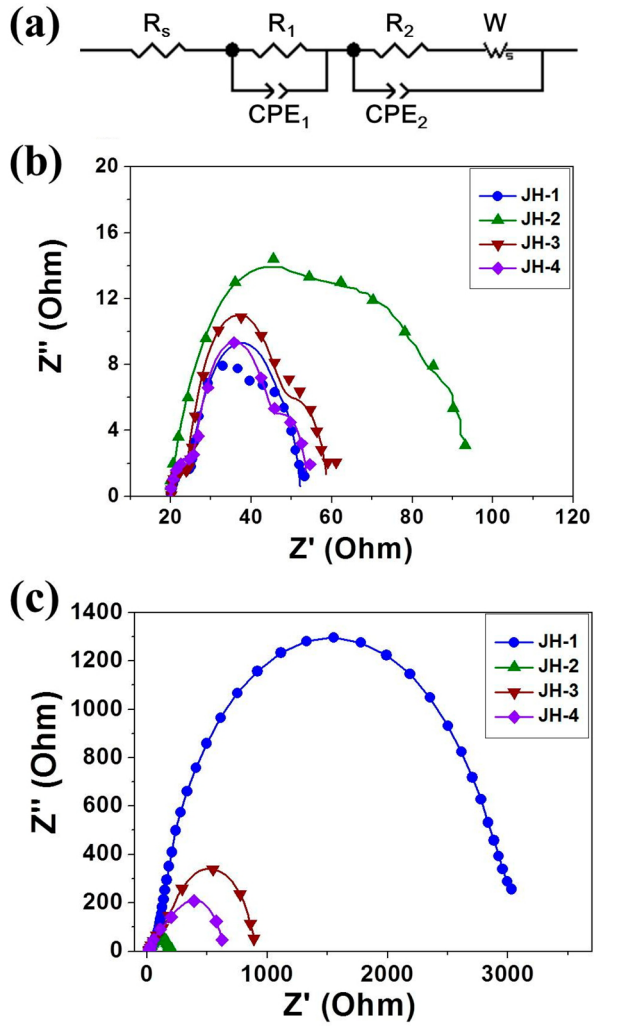

Figure 6. (a) Equivalent circuit model and Nyquist plots of the DSSCs based on the dyes under 100 mW cm^{-2} illumination (b) and in the dark (c).

EIS Analysis. EIS is commonly used to characterize the kinetics of the DSSC by analyzing the variation in the impedance associated with different interfaces of the cells.[53] In this work, the Nyquist plots were measured at the V_{oc} of the DSSCs under 1.5 AM full sunlight, and under a forward bias of 0.55 V in the dark, respectively, as shown in Figure 6b and c. The Nyquist plots of the DSSCs are fitted with Z-view software using appropriate equivalent circuit model shown in Figure 6a. From low to high impedance, the two semicircles correspond to the resistance (R1) at Pt/electrolyte interface and the resistance (R2) at the TiO_2 film/electrolyte interface. R1 values are similar for all dyes, as Pt counter electrode was used in all cases. The R2 value depends on the competition between regeneration of iodide/triiodide by the redox couple, charge transport, and charge recombination of the electrons injected into the TiO_2 conduction band with the oxidized dyes or electrolytes. The rate of regeneration is normally faster than that of the charge recombination. Under illumination condition, JH-2 is found to have the largest R2 values (70.4 Ω) than the others (16.9−34.0 Ω), as shown in Figure 6b, where the electron transfer rate of JH-2 at the TiO_2 and electrolyte interface have shifted to a higher frequency (f) as shown in the Bode phase plot (Supporting Information Figure S7). The electron lifetime (τ_r), estimated from the equation, $\tau_r = 1/(2\pi f)$, decreases in order of JH-1 (13.37 ms) > JH-3 (11.05 ms)

Table 2. DSSCs Performance Parameters of the Dyes and with or without Coadsorbent of 10 mM CDCA

dye	J_{sc} (mA/cm^2)	V_{oc} (V)	*ff*	PCE (%)	dye loading (μmol/cm^2)
JH-1	12.60 ± 0.35	0.70 ± 0.02	0.71 ± 0.04	6.18 ± 0.10	0.15
JH-1/CDCA	12.86 ± 0.24	0.72 ± 0.02	0.72 ± 0.01	6.65 ± 0.03	0.15
JH-2	3.23 ± 0.46	0.60 ± 0.05	0.72 ± 0.02	1.42 ± 0.35	0.22
JH-2/CDCA	4.36 ± 0.94	0.63 ± 0.03	0.69 ± 0.02	1.91 ± 0.45	0.18
JH-3	10.92 ± 0.30	0.69 ± 0.01	0.70 ± 0.02	5.27 ± 0.07	0.18
JH-3/CDCA	11.44 ± 0.18	0.71 ± 0.01	0.69 ± 0.02	5.60 ± 0.12	0.17
JH-4	12.43 ± 0.63	0.68 ± 0.01	0.72 ± 0.02	5.98 ± 0.13	0.20
JH-4/CDCA	14.29 ± 0.24	0.70 ± 0.01	0.73 ± 0.01	7.33 ± 0.01	0.17
N719	15.05 ± 0.30	0.76 ± 0.01	0.66 ± 0.01	7.56 ± 0.03	

> JH-4 (7.51 ms) > JH-2 (0.73 ms). Shorter electron lifetime of DSSC with JH-2 implies that the charge injected into the TiO_2 conduction band more readily recombine with the oxidized dye or I_3^- ions. As aforementioned, the higher HOMO level of JH-2 (vide supra) likely retards dye regeneration and leads to more electron recombination with the oxidized dye. In both cases, a lower J_{sc} value and IPCE are expected, as observed.

In the dark condition, the R2′ value of the DSSCs decreases in the order of JH-1 (3005.6 Ω) > JH-3 (695.2 Ω) > JH-4 (428.9 Ω) > JH-2 (147.5 Ω), which is consistent with the order of V_{oc} value. More planar arylamine donor (JH-2 and JH-4) seems to be less effective in dark current suppression. Dark current suppression also appears to be less efficient for the dye with a longer skeleton (JH-3).

Device Performance with Coabsorbed CDCA. It is common to add coadsorbent during dye soaking to improve the cell efficiency for two purposes: (1) antiaggregation of the dyes due to dilution effect; (2) dark current suppression due to coverage of exposed TiO_2 surface.[54,55] Therefore, we also tested DSSCs with 10 mM of chenodeoxycholic acid (CDCA) as the coadsorbent though *J*-aggregation of the JH dyes was found to have contribution to the solar light-to-electricity conversion at the longer wavelength (vide supra). This observation suggests that addition of CDCA mainly removes those aggregates harmful to electron injection, such as dyes not anchored on TiO_2. The *J*−*V* plots and IPCE spectra are shown in Figure 7, and the relevant data are listed in Table 2.

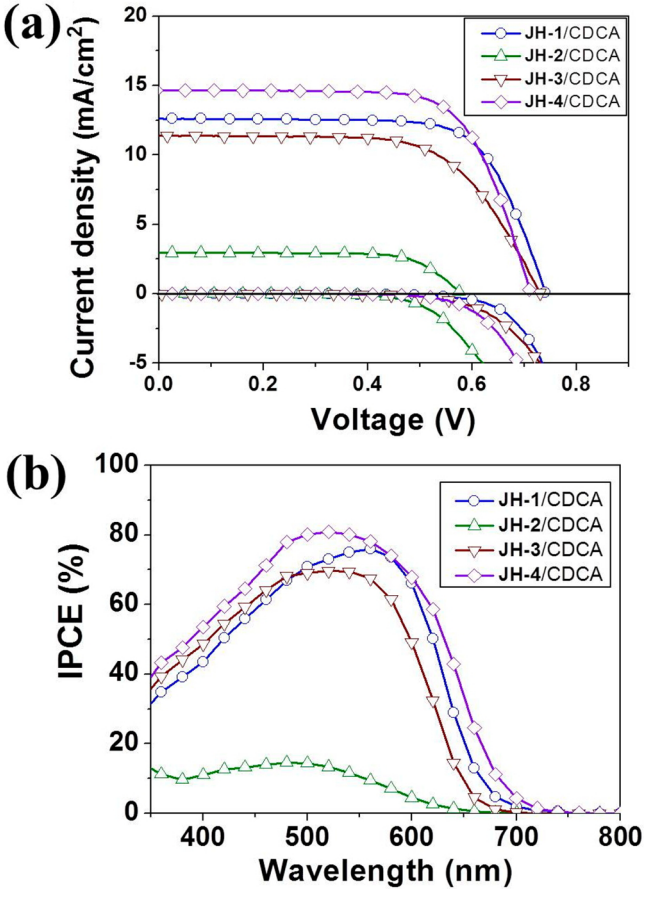

Figure 7. *J*−*V* curves (a) and IPCE plots (b) of DSSCs based on the dyes with CDCA as coabsorbent (10 mM).

The efficiencies of all the DSSCs have been improved, and they decrease in the order of JH-4 (7.33%) > JH-1 (6.65%) > JH-3 (5.60%) > JH-2 (1.91%). The cell efficiencies of JH-4 and JH-1 reach 97 and 88% of N719-based standard cell (7.56%), respectively. Both V_{oc} and J_{sc} values were increased upon addition of CDCA for all dyes, suggesting that CDCA helped with alleviation of dye aggregation and/or dark current suppression. Dark current suppression is more evident for JH-3 and JH-4 upon CDCA addition based on prominent increment of the recombination resistance in the dark (EIS in the dark, see Figure 8b) for JH-3 (1705.1 Ω vs 695.2 Ω) and

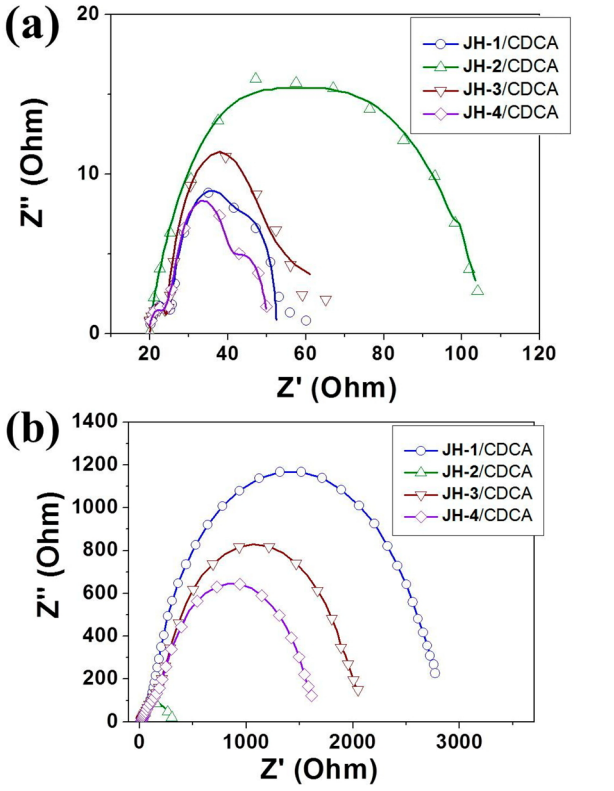

Figure 8. Nyquist plots of the DSSCs based on the dyes with CDCA as coabsorbent (10 mM) under 100 mW cm^{-2} illumination (a) and in the dark (b).

JH-4 (1342.1 Ω vs 428.9 Ω). It is interesting to note that the PCE values are higher for JH-3 and JH-4 from ∼500 nm and above when CDCA is added. This observation suggests that addition of CDCA mainly removes those aggregates harmful to electron injection. The J_{sc} value decreases slightly for JH-1, indicating 10 mM of CDCA is already high enough to compete with the dye for the TiO_2 adsorption sites.

CONCLUSIONS

Dipolar metal-free organic dyes containing a rigid planar entity possessing both electron rich and electron deficient units, dithieno[3′,2′:3,4;2″,3″:5,6]benzo[1,2-*c*]furazan (DTBF), have been synthesized and successfully used as the sensitizers for dye-sensitized solar cells (DSSCs). *J*-aggregation of the dyes in the film state contributes to the photocurrent, and the cells exhibit good conversion efficiency up to ∼82% of N719-based standard DSSC (7.56%). Upon addition of CDCA as the coadsorbent, the best cell efficiency can be boosted to 7.33%, which is close to that of the standard cell.

dx.doi.org/10.1021/am5067145 | ACS Appl. Mater. Interfaces 2014, 6, 22612−22621

■ ASSOCIATED CONTENT

Supporting Information

Absorption spectra with and without CDCA coadsorbent on TiO_2 films (Figures S1 and S2), normalized absorption and photoluminescence spectra (Figure S3), cyclic voltammogram (Figure S4), frontier orbitals (Figure S5), and dihedral angles (Figure S6), Bode plots (Figure S7), and calculated low-lying transition (Table S1) data. This material is available free of charge via the Internet at http://pubs.acs.org.

■ AUTHOR INFORMATION

Corresponding Author

*E-mail: jtlin@chem.sinica.edu.tw.

Author Contributions

The manuscript was written through contributions of all authors. All authors have given approval to the final version of the manuscript.

Notes

The authors declare no competing financial interest.

■ ACKNOWLEDGMENTS

Financial support of this research by Academia Sinica (AS) and Ministry of Science and Technology (MST, Taiwan) are gratefully acknowledged. Support from the Instrumental Center of Institute of Chemistry (AS) is also acknowledged.

■ REFERENCES

(1) O'Regan, B.; Grätzel, M. A Low-Cost, High-Efficiency Solar Cell Based on Dye-Sensitized Colloidal TiO_2 films. *Nature* **1991**, *353*, 737−740.

(2) Grätzel, M. Photoelectrochemical Cells. *Nature* **2001**, *414*, 338−344.

(3) Chen, C.-Y.; Wang, M.; Li, J.-Y.; Pootrakulchote, N.; Alibabaei, L.; Ngoc-le, C.-h.; Decoppet, J.-D.; Tsai, J.-H.; Grätzel, C.; Wu, C.-G.; Zakeeruddin, S. M.; Grätzel, M. Highly Efficient Light-Harvesting Ruthenium Sensitizer for Thin-Film Dye-Sensitized Solar Cells. *ACS Nano* **2009**, *3*, 3103−3109.

(4) Gao, F.; Wang, Y.; Shi, D.; Zhang, J.; Wang, M.; Jing, X.; Humphry-Baker, R.; Wang, P.; Zakeeruddin, S. M.; Grätzel, M. Enhance the Optical Absorptivity of Nanocrystalline TiO_2 Film with High Molar Extinction Coefficient Ruthenium Sensitizers for High Performance Dye-Sensitized Solar Cells. *J. Am. Chem. Soc.* **2008**, *130*, 10720−10728.

(5) Mathew, S.; Yella, A.; Gao, P.; Humphry-Baker, R.; Curchod, B. F.; Ashari-Astani, N.; Tavernelli, I.; Rothlisberger, U.; Nazeeruddin, M. K.; Gratzel, M. Dye-Sensitized Solar Cells with 13% Efficiency Achieved Through the Molecular Engineering of Porphyrin Sensitizers. *Nat. Chem.* **2014**, *6*, 242−247.

(6) Yella, A.; Mai, C. L.; Zakeeruddin, S. M.; Chang, S. N.; Hsieh, C. H.; Yeh, C. Y.; Gratzel, M. Molecular Engineering of Push-Pull Porphyrin Dyes for Highly Efficient Dye-Sensitized Solar Cells: The Role of Benzene Spacers. *Angew. Chem., Int. Ed.* **2014**, *53*, 2973−2977.

(7) Yang, J.; Ganesan, P.; Teuscher, J.; Moehl, T.; Kim, Y. J.; Yi, C.; Comte, P.; Pei, K.; Holcombe, T. W.; Nazeeruddin, M. K.; Hua, J.; Zakeeruddin, S. M.; Tian, H.; Gratzel, M. Influence of the Donor Size in D−π−A Organic Dyes for Dye-Sensitized Solar Cells. *J. Am. Chem. Soc.* **2014**, *136*, 5722−5730.

(8) Liang, M.; Chen, J. Arylamine Organic Dyes for Dye-Sensitized Solar Cells. *Chem. Soc. Rev.* **2013**, *42*, 3453−3488.

(9) Wu, Y.; Zhu, W. Organic Sensitizers from D−π−A to D−A−π−A: Effect of the Internal Electron-Withdrawing Units on Molecular Absorption, Energy Levels, and Photovoltaic Performances. *Chem. Soc. Rev.* **2013**, *42*, 2039−2058.

(10) Yen, Y. S.; Lee, C. T.; Hsu, C. Y.; Chou, H. H.; Chen, Y. C.; Lin, J. T. Benzotriazole-Containing D−π−A Conjugated Organic Dyes for Dye-Sensitized Solar Cells. *Chem.—Asian J.* **2013**, *8*, 809−816.

(11) Chou, H.-H.; Chen, Y.-C.; Huang, H.-J.; Lee, T.-H.; Lin, J. T.; Tsai, C.; Chen, K. High-Performance Dye-Sensitized Solar Cells based on 5,6-Bis-hexyloxy-benzo[2,1,3]thiadiazole. *J. Mater. Chem.* **2012**, *22*, 10929−10938.

(12) Velusamy, M.; Hsu, Y. C.; Lin, J. T.; Chang, C. W.; Hsu, C. P. 1-Alkyl-1*H*-imidazole-Based Dipolar Organic Compounds for Dye-Sensitized Solar Cells. *Chem.—Asian J.* **2010**, *5*, 87−96.

(13) Hung, W. I.; Liao, Y. Y.; Hsu, C. Y.; Chou, H. H.; Lee, T. H.; Kao, W. S.; Lin, J. T. High-Performance Dye-Sensitized Solar Cells Based on Phenothiazine Dyes Containing Double Anchors and Thiophene Spacers. *Chem.—Asian J.* **2014**, *9*, 357−366.

(14) Wu, Y.; Marszalek, M.; Zakeeruddin, S. M.; Zhang, Q.; Tian, H.; Grätzel, M.; Zhu, W. High-Conversion-Efficiency Organic Dye-Sensitized Solar Cells: Molecular Engineering on D−A−π−A Featured Organic Indoline Dyes. *Energy Environ. Sci.* **2012**, *5*, 8261−8272.

(15) Zhu, H.; Li, W.; Wu, Y.; Liu, B.; Zhu, S.; Li, X.; Ågren, H.; Zhu, W. Insight into Benzothiadiazole Acceptor in D−A−π−A Configuration on Photovoltaic Performances of Dye-Sensitized Solar Cells. *ACS Sustainable Chem. Eng.* **2014**, *2*, 1026−1034.

(16) Li, H.; Wu, Y.; Geng, Z.; Liu, J.; Xu, D.; Zhu, W. Co-Sensitization of Benzoxadiazole based D−A−π−A Featured Sensitizers: Compensating Light-Harvesting and Retarding Charge Recombination. *J. Mater. Chem. A* **2014**, *2*, 14649−14657.

(17) Chaurasia, S.; Hung, W. I.; Chou, H. H.; Lin, J. T. Incorporating a New 2*H*-[1,2,3]Triazolo[4,5-*c*]pyridine Moiety to Construct D−A−π−A Organic Sensitizers for High Performance Solar Cells. *Org. Lett.* **2014**, *16*, 3052−3055.

(18) Zeng, J.; Zhang, T.; Zang, X.; Kuang, D.; Meier, H.; Cao, D. D−A−π−A Organic Sensitizers Containing a Benzothiazole Moiety as an Additional Acceptor for Use in Solar Cells. *Sci. China: Chem.* **2012**, *56*, 505−513.

(19) Qu, S.; Qin, C.; Islam, A.; Hua, J.; Chen, H.; Tian, H.; Han, L. Tuning the Electrical and Optical Properties of Diketopyrrolopyrrole Complexes for Panchromatic Dye-Sensitized Solar Cells. *Chem.—Asian J.* **2012**, *7*, 2895−2903.

(20) Zhang, F.; Jiang, K.-J.; Huang, J.-H.; Yu, C.-C.; Li, S.-G.; Chen, M.-G.; Yang, L.-M.; Song, Y.-L. A Novel Compact DPP Sye with Enhanced Light Harvesting and Charge Transfer Properties for Highly Efficient DSCs. *J. Mater. Chem. A* **2013**, *1*, 4858−4863.

(21) Yum, J. H.; Holcombe, T. W.; Kim, Y.; Rakstys, K.; Moehl, T.; Teuscher, J.; Delcamp, J. H.; Nazeeruddin, M. K.; Gratzel, M. Blue-Colored Highly Efficient Dye-Sensitized Solar Cells by Implementing the Diketopyrrolopyrrole Chromophore. *Sci. Rep.* **2013**, *3*, 2446.

(22) Ying, W.; Zhang, X.; Li, X.; Wu, W.; Guo, F.; Li, J.; Ågren, H.; Hua, J. Synthesis and Photovoltaic Properties of new [1,2,5]-Thiadiazolo[3,4-*c*]pyridine-Based Organic Broadly Absorbing Sensitizers for Dye-Sensitized Solar Cells. *Tetrahedron* **2014**, *70*, 3901−3908.

(23) Chaurasia, S.; Hsu, C.-Y.; Chou, H.-H.; Lin, J. T. Synthesis, Optical and Electrochemical Properties of Pyridal[2,1,3]thiadiazole Based Organic Dyes for Dye Sensitized Solar Cells. *Org. Electron.* **2014**, *15*, 378−390.

(24) Ying, W.; Yang, J.; Wielopolski, M.; Moehl, T.; Moser, J.-E.; Comte, P.; Hua, J.; Zakeeruddin, S. M.; Tian, H.; Grätzel, M. New Pyrido[3,4-*b*]pyrazine-Based Sensitizers for Efficient and Stable Dye-Sensitized Solar Cells. *Chem. Sci.* **2014**, *5*, 206−214.

(25) Pei, K.; Wu, Y.; Islam, A.; Zhang, Q.; Han, L.; Tian, H.; Zhu, W. Constructing High-Efficiency D−A−π−A-Featured Solar Cell Sensitizers: A Promising Building Block of 2,3-Diphenylquinoxaline for Antiaggregation and Photostability. *ACS Appl. Mater. Interfaces* **2013**, *5*, 4986−4995.

(26) Li, S. R.; Lee, C. P.; Yang, P. F.; Liao, C. W.; Lee, M. M.; Su, W. L.; Li, C. T.; Lin, H. W.; Ho, K. C.; Sun, S. S. Structure-Performance Correlations of Organic Dyes with an Electron-Deficient Diphenylquinoxaline Moiety for Dye-Sensitized Solar Cells. *Chem.—Eur. J.* **2014**, *20*, 10052−10064.

(27) Ying, W.; Guo, F.; Li, J.; Zhang, Q.; Wu, W.; Tian, H.; Hua, J. Series of New D−A−π−A Organic Broadly Absorbing Sensitizers Containing Isoindigo Unit for Highly Efficient Dye-Sensitized Solar Cells. *ACS Appl. Mater. Interfaces* **2012**, *4*, 4215−4224.
(28) Li, S. G.; Jiang, K. J.; Huang, J. H.; Yang, L. M.; Song, Y. L. Molecular Engineering of Panchromatic Isoindigo Sensitizers for Dye-Sensitized Solar Cell Applications. *Chem. Commun.* **2014**, *50*, 4309−4311.
(29) Yen, Y.-S.; Lin, T.-Y.; Hsu, C.-Y.; Chen, Y.-C.; Chou, H.-H.; Tsai, C.; Lin, J. T. A Remarkable Enhancement of Efficiency by Co-Adsorption with CDCA on the Bithiazole-Based Dye-Sensitized Solar Cells. *Org. Electron.* **2013**, *14*, 2546−2554.
(30) Chang, Y. J.; Chow, T. J. Highly Efficient Triarylene Conjugated Dyes for Sensitized Solar Cells. *J. Mater. Chem.* **2011**, *21*, 9523−9531.
(31) Kang, X.; Zhang, J.; Rojas, A. J.; O'Neil, D.; Szymanski, P.; Marder, S. R.; El-Sayed, M. A. Deposition of Loosely Bound Organic D−A−π−A′ Dyes on Sensitized TiO_2 Film: A Possible Strategy to Suppress Charge Recombination and Enhance Power Conversion Efficiency in Dye-Sensitized Solar Cells. *J. Mater. Chem. A* **2014**, *2*, 11229−11234.
(32) Arroyave, F. A.; Richard, C. A.; Reynolds, J. R. Efficient Synthesis of Benzo[1,2-b:6,5-*b*′]dithiophene-4,5-dione (BDTD) and Its Chemical Transformations into Precursors for π-Conjugated Materials. *Org. Lett.* **2012**, *14*, 6138−6141.
(33) Huang, Z.-S.; Feng, H.-L.; Zang, X.-F.; Iqbal, Z.; Zeng, H.; Kuang, D.-B.; Wang, L.; Meier, H.; Cao, D. Dithienopyrrolobenzothiadiazole-Based Organic Dyes for Efficient Dye-Sensitized Solar Cells. *J. Mater. Chem. A* **2014**, *2*, 15365−15376.
(34) Kusama, H.; Sugihara, H.; Sayama, K. Effect of Cations on the Interactions of Ru Dye and Iodides in Dye-Sensitized Solar Cells: A Density Functional Theory Study. *J. Phys. Chem. C* **2011**, *115*, 2544−2552.
(35) Tuikka, M.; Hirva, P.; Rissanen, K.; Korppi-Tommola, J.; Haukka, M. Halogen Bonding—A Key Step in Charge Recombination of the Dye-Sensitized Solar Cell. *Chem. Commun.* **2011**, *47*, 4499−4501.
(36) Kusama, H.; Sayama, K. Effect of Side Groups for Ruthenium Bipyridyl Dye on the Interactions with Iodine in Dye-Sensitized Solar Cells. *J. Phys. Chem. C* **2012**, *116*, 1493−1502.
(37) Nitani, M.; Ie, Y.; Tada, H.; Aso, Y. Solution-Processable n-Type Organic Field-Effect Transistor (OFET) Materials Based on Carbonyl-Bridged Bithiazole and Dioxocyclopentene-Annelated Thiophenes. *Chem.—Asian J.* **2011**, *6*, 2352−2361.
(38) Chen, Y. C.; Chen, Y. H.; Chou, H. H.; Chaurasia, S.; Wen, Y. S.; Lin, J. T.; Yao, C. F. Naphthyl and Thienyl Units as Bridges for Metal-Free Dye-Sensitized Solar Cells. *Chem.—Asian J.* **2012**, *7*, 1074−1084.
(39) Chen, C. H.; Hsu, Y. C.; Chou, H. H.; Thomas, K. R.; Lin, J. T.; Hsu, C. P. Dipolar Compounds Containing Fluorene and a Heteroaromatic Ring as the Conjugating Bridge for High-Performance Dye-Sensitized Solar Cells. *Chem.—Eur. J.* **2010**, *16*, 3184−3193.
(40) Chang, Y.-C.; Yeh, S.-C.; Chen, Y.-H.; Chen, C.-T.; Lee, R.-H.; Jeng, R.-J. New Carbazole-Substituted Anthracene Derivatives Based Nondoped Blue Light-Emitting Devices with High Brightness and Efficiency. *Dyes Pigm.* **2013**, *99*, 577−587.
(41) Vaswani, H. M.; Hsu, C.-P.; Head-Gordon, M.; Fleming, G. R. Quantum Chemical Evidence for an Intramolecular Charge-Transfer State in the Carotenoid Peridinin of Peridinin−Chlorophyll−Protein. *J. Phys. Chem. B* **2003**, *107*, 7940−7946.
(42) Kurashige, Y.; Nakajima, T.; Kurashige, S.; Hirao, K.; Nishikitani, Y. Theoretical Investigation of the Excited States of Coumarin Dyes for Dye-Sensitized Solar Cells. *J. Phys. Chem. A* **2007**, *111*, 5544−5548.
(43) Dreuw, A.; Head-Gordon, M. Failure of Time-Dependent Density Functional Theory for Long-Range Charge-Transfer Excited States: The Zincbacteriochlorin−Bacteriochlorin and Bacteriochlorophyll−Spheroidene Complexes. *J. Am. Chem. Soc.* **2004**, *126*, 4007−4016.
(44) Sonar, P.; Williams, E. L.; Singh, S. P.; Dodabalapur, A. Thiophene−Benzothiadiazole−Thiophene (D−A−D) Based Polymers: Effect of Donor/Acceptor Moieties Adjacent to D−A−D Segment on Photophysical and Photovoltaic Properties. *J. Mater. Chem.* **2011**, *21*, 10532−10541.
(45) Lu, X.; Jia, X.; Wang, Z.-S.; Zhou, G. X-Shaped Organic Dyes with a Quinoxaline Bridge for Use in Dye-Sensitized Solar Cells. *J. Mater. Chem. A* **2013**, *1*, 9697−9706.
(46) Yang, H.-Y.; Yen, Y.-S.; Hsu, Y.-C.; Chou, H.-H.; Lin, J. T. Organic Dyes Incorporating the Dithieno[3,2-*b*:2′,3′-*d*]thiophene Moiety for Efficient Dye-Sensitized Solar Cells. *Org. Lett.* **2010**, *12*, 16−19.
(47) Li, S.-L.; Jiang, K.-J.; Shao, K.-F.; Yang, L.-M. Novel Organic Dyes for Efficient Dye-Sensitized Solar Cells. *Chem. Commun.* **2006**, 2792−2794.
(48) Hoke, E. T.; Sachs-Quintana, I. T.; Lloyd, M. T.; Kauvar, I.; Mateker, W. R.; Nardes, A. M.; Peters, C. H.; Kopidakis, N.; McGehee, M. D. The Role of Electron Affinity in Determining Whether Fullerenes Catalyze or Inhibit Photooxidation of Polymers for Solar Cells. *Adv. Energy Mater.* **2012**, *2*, 1351−1357.
(49) Chen, Y. C.; Chou, H. H.; Tsai, M. C.; Chen, S. Y.; Lin, J. T.; Yao, C. F.; Chen, K. Thieno[3,4-*b*]thiophene-based Organic Dyes for Dye-Sensitized Solar Cells. *Chem.—Eur. J.* **2012**, *18*, 5430−5437.
(50) Hara, K.; Sato, T.; Katoh, R.; Furube, A.; Ohga, Y.; Shinpo, A.; Suga, S.; Sayama, K.; Sugihara, H.; Arakawa, H. Molecular Design of Coumarin Dyes for Efficient Dye-Sensitized Solar Cells. *J. Phys. Chem. B* **2003**, *107*, 597−606.
(51) Huang, S. T.; Hsu, Y. C.; Yen, Y. S.; Chou, H. H.; Lin, J. T.; Chang, C. W.; Hsu, C. P.; Tsai, C.; Yin, D. J. Organic Dyes Containing a Cyanovinyl Entity in the Spacer for Solar Cells Applications. *J. Phys. Chem. C* **2008**, *112*, 19739−19747.
(52) Planells, M.; Pellejà, L.; Clifford, J. N.; Pastore, M.; De Angelis, F.; López, N.; Marder, S. R.; Palomares, E. Energy Levels, Charge Injection, Charge Recombination, and Dye Regeneration Dynamics for Donor−Acceptor π-Conjugated Organic Dyes in Mesoscopic TiO_2 Sensitized Solar Cells. *Energy Environ. Sci.* **2011**, *4*, 1820−1829.
(53) Benkstein, K. D.; Kopidakis, N.; Lagemaat, J. v. d.; Frank, A. J. Influence of the Percolation Network Geometry on Electron Transport in Dye-Sensitized Titanium Dioxide Solar Cells. *J. Phys. Chem. B* **2003**, *107*, 7759−7767.
(54) Zhang, S.; Yang, X.; Qin, C.; Numata, Y.; Han, L. Interfacial Engineering for Dye-Sensitized Solar Cells. *J. Mater. Chem. A* **2014**, *2*, 5167−5177.
(55) Li, J.; Wu, W.; Yang, J.; Tang, J.; Long, Y.; Hua, J. Effect of Chenodeoxycholic Acid (CDCA) Additive on Phenothiazine Dyes Sensitized Photovoltaic Performance. *Sci. China: Chem.* **2011**, *54*, 699−706.